

A BLOCK-ACOUSTIC PRECONDITIONER FOR THE ELASTIC HELMHOLTZ EQUATION *

RACHEL YOVEL[†] AND ERAN TREISTER[†]

Abstract. We present a novel block-preconditioner for the elastic Helmholtz equation, based on a reduction to acoustic Helmholtz equations. Both versions of the Helmholtz equations are challenging numerically. The elastic Helmholtz equation is larger, as a system of PDEs, and harder to solve due to its more complicated physics. It was recently suggested that the elastic Helmholtz equation can be reformulated as a generalized saddle-point system, opening the door to the current development. Utilizing the approximate commutativity of the underlying differential operators, we suggest a block-triangular preconditioner whose diagonal blocks are acoustic Helmholtz operators. Thus, we enable the solution of the elastic version using virtually any existing solver for the acoustic version as a black-box. We prove a sufficient condition for the convergence of our method, that sheds light on the long questioned role of the commutator in the convergence of approximate commutator preconditioners. We show scalability of our preconditioner with respect to the Poisson ratio and with respect to the grid size. We compare our approach, combined with multigrid solve of each block, to a recent monolithic multigrid method for the elastic Helmholtz equation. The block-acoustic multigrid achieves a lower computational cost for various heterogeneous media, and a significantly lower memory consumption, compared to the monolithic approach. It results in a fast solution method for wave propagation problems in challenging heterogeneous media in 2D and 3D.

Key words. Elastic wave modeling, elastic Helmholtz equation, saddle-point systems, block preconditioning, approximate commutators.

MSC codes. 65N22, 74B99, 35J05, 65F10, 65F30

1. Introduction. The Helmholtz equations model wave propagation in the frequency domain. The acoustic Helmholtz equation models acoustics [61, 15] and electromagnetic waves [66], whereas the elastic Helmholtz equation models waves in solid media, such as earth subsurface [62]. Both versions are difficult for numerical solution, and counted as open problems. The resulting linear systems are complex, indefinite, and large, since discretizing high-frequency waves requires very fine meshes. The elastic equation amplifies these difficulties over the acoustic one: as a system of equations, it is larger, and the more complicated physics — including both shear and pressure waves — gives rise to the need for special care.

Many solvers and preconditioners were suggested for the acoustic Helmholtz equation, including geometric and algebraic multigrid methods [25, 42, 43, 39, 58, 14], domain decomposition methods [26, 54, 57, 64, 34], deflation methods [13], deep learning methods [3], and other methods [30, 29, 60]. Yet, just a few solvers are available for the elastic version [46, 4, 9], most of which are multigrid based. In [55], a monolithic multigrid solver is proposed, achieving scalability with respect to the Poisson ratio. A main ingredient in the method suggested there is the introduction of a mixed formulation for the elastic Helmholtz equation. That is, writing the equation as a generalized saddle-point system with an indefinite leading block. This formulation opens the door to specifically tailored block preconditioners for the elastic Helmholtz equation.

There is an abundance of research on block preconditioners for saddle-point systems, especially in the context of incompressible fluid flow. For a comprehensive

*Corresponding author: Rachel Yovel.

Funding: This research was supported by The Israel Science Foundation (grant No. 656/23). RY is supported by the Ariane de Rothschild scholarship and by Kreitman High-tech scholarship. The authors also thank the Lynn and William Frankel Center for Computer Science at BGU.

[†]Ben-Gurion University, Beer Sheva, Israel. yovelr@bgu.ac.il, erant@cs.bgu.ac.il

overview, see the review [5], Chapter 9 in the book [22], and references therein. A main approach is the block-diagonal or block-triangular Schur-complement preconditioners, based on a block elimination of the given system. Eigenvalue bounds for Schur-complement preconditioners are given in [41, 2], extended in [35] to the non-symmetric case. However, forming and inverting the Schur-complement is very costly, and broad research in the last decades is dedicated to the search of cheap approximations for the inverse of the Schur-complement.

One way to approximate the inverse Schur-complement is based on the notion of approximate commutators [19, 52, 16, 18, 23, 44], that was suggested in the context of incompressible fluid flow. The F_p , or pressure convection-diffusion (PCD) preconditioner [20], creates an approximation of the leading block by re-discretizing it on the pressure space. The BFBt, or least squares commutator (LSC) preconditioner [20, 18], is based on a more algebraic observation: seeking an approximation for the leading block in the pressure's space that will minimize the commutator in a least squares sense. Weighted adaptations of the BFBt preconditioner directed to Stokes-like systems with variable viscosity were suggested in [47, 48]. Some Schur-complement-free preconditioners were also suggested, directly utilizing the commutation relations to prevent the inversion of the leading block, see the pressure-Poisson approach [51, 36].

However, most of the research in this direction is dedicated to incompressible fluid flow problems, which are different in nature from the elastic Helmholtz equation. First, the elastic Helmholtz equation typically deals with compressible materials. Algebraically speaking, the resulting saddle-point matrix for the elastic Helmholtz equation has a nonzero regularization block, regardless of the discretization. Second, the leading block is indefinite. There is some literature on the non-SPD case, e.g., the well-known augmented Lagrangian approach [28, 6], that deals with the case of a singular leading block. To the best of our knowledge, no approximate commutator preconditioners were suggested for generalized saddle-point systems with an indefinite leading block, prior to this work.

In this work, we present a Schur-complement-free approximate commutator preconditioner. Our block-acoustic preconditioner is block-triangular, and its diagonal blocks are acoustic Helmholtz operators. Reducing a large, coupled problem into smaller decoupled problems, enhances the efficiency and introduces natural parallelization. Moreover, this reduction-based framework enables the use of any advanced solver for acoustic Helmholtz within the solution of the elastic version. Our preconditioner scales well with respect to the Poisson ratio, and given a direct solve of each block, is also scalable with respect to the grid size. We combine our preconditioner with a multigrid solve of each block, and show that it outperforms monolithic multigrid, for real world geophysical problems in 2D and 3D.

The paper is organized as follows: in Section 2 we give mathematical background, including multigrid methods and approximate commutator preconditioners. In Section 3 we derive the method and prove a theoretical result, shedding light on the role of the commutator in our method. In Section 4 we test our method numerically, and finally, in Section 5 we give concluding remarks and discuss future work.

2. Background. In this section we present the acoustic and elastic Helmholtz equations. Furthermore, we give some general background on multigrid and specifically on the multigrid methods for the Helmholtz equations that we use in this work. Finally, we give some background on approximate commutator preconditioning.

2.1. The acoustic and elastic Helmholtz equation. Let $p = p(\vec{x})$, $\vec{x} \in \Omega$ be the Fourier transform of the wave's pressure field, let $\omega = 2\pi f$ be the angular

frequency, $\kappa = \kappa(\vec{x}) > 0$ the “slowness” of the wave in the medium (the inverse of the wave velocity). Let $\rho = \rho(\vec{x}) > 0$ be the density of the medium and $q(\vec{x})$ the source of the waves. Then the acoustic Helmholtz equation is given by

$$(2.1) \quad \rho \nabla \cdot (\rho^{-1} \nabla p) + \omega^2 \kappa^2 \left(1 - \frac{\gamma}{\omega} \iota\right) p = q$$

where ι stands for the imaginary unit and γ represents the physical attenuation. To solve this equation numerically, we discretize it in a finite domain by a finite differences scheme. It is usually equipped with absorbing boundary conditions (ABC) [24] or perfectly matched layers (PML) [7, 53, 32, 45], to mimic the propagation of a wave in an open domain, and to avoid reflections from the boundary.

The elastic Helmholtz equation in an isotropic medium is given by

$$(2.2) \quad \nabla \lambda \nabla \cdot \vec{u} + \vec{\nabla} \cdot \mu \left(\vec{\nabla} \vec{u} + \vec{\nabla} \vec{u}^T \right) + \rho \omega^2 \left(1 - \frac{\gamma}{\omega} \iota\right) \vec{u} = \vec{q}_s$$

where $\vec{u} = \vec{u}(\vec{x})$ is the displacement vector, or by the following formulation¹

$$(2.3) \quad \nabla(\lambda + \mu) \nabla \cdot \vec{u} + \vec{\nabla} \cdot \mu \vec{\nabla} \vec{u} + \rho \omega^2 \left(1 - \frac{\gamma}{\omega} \iota\right) \vec{u} = \vec{q}_s,$$

where $\lambda = \lambda(\vec{x})$ and $\mu = \mu(\vec{x})$ are the Lamé coefficients, that represents the stress-strain relationship in the material. These coefficient determine the pressure wave velocity $V_p = \sqrt{(\lambda + 2\mu)/\rho}$ and the shear wave velocity $V_s = \sqrt{\mu/\rho}$, see e.g. [38]. The Poisson ratio is given by $\sigma = \lambda/2(\lambda + \mu)$, and describes deformation properties of the material. For most materials, $0 < \sigma < 0.5$, and in the nearly incompressible case (that is counted as the most difficult case), $\sigma \rightarrow 0.5$ or $\lambda \gg \mu$.

In the incompressible case, the elastic Helmholtz equation is reducible to the acoustic Helmholtz equation: substituting $\mu = 0$ in (2.3) and applying $\rho \nabla \cdot \rho^{-1}$ on both sides, yields

$$(2.4) \quad \rho \nabla \cdot \rho^{-1} \nabla \lambda (\nabla \cdot \vec{u}) + \frac{\rho \omega^2}{\lambda} \left(1 - \frac{\gamma}{\omega} \iota\right) \lambda \nabla \cdot \vec{u} = \rho \nabla \cdot \rho^{-1} \vec{q}_s.$$

That is, an acoustic Helmholtz equation, similar to (2.1), with $\lambda \nabla \cdot \vec{u}$ as the unknown scalar function. Note that the wave velocity of (2.4) is equal to the pressure wave velocity of the original equation, (2.3). Such a reduction is the core idea behind our method. However, the reduction above is possible (and exact), only when $\mu = 0$, the material is incompressible and there are no shear waves. A similar reduction in the compressible case is less trivial, as it involves both shear and pressure wave velocities.

The mixed formulation, originally suggested for linear elasticity problems [27, 65] and recently suggested for the elastic Helmholtz equation [55], is derived as follows. By introducing a new pressure variable $p = -(\lambda + \mu) \nabla \cdot \vec{u}$ and substituting it in (2.3), we have

$$(2.5) \quad \begin{pmatrix} -\vec{\nabla} \cdot \mu \vec{\nabla} - \rho \omega^2 \left(1 - \frac{\gamma}{\omega} \iota\right) & \nabla \\ -\nabla \cdot & -\frac{1}{\lambda + \mu} \end{pmatrix} \begin{pmatrix} \vec{u} \\ p \end{pmatrix} = \begin{pmatrix} -\vec{q}_s \\ 0 \end{pmatrix}.$$

We discretize (2.5) using a marker and cell (MAC) discretization [33] with standard second-order finite difference stencil. We locate the displacement components $\mathbf{u}_1, \mathbf{u}_2$

¹The two formulations are equivalent in homogeneous media, and resembles each other well for heterogeneous media.

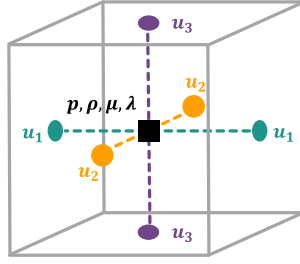


FIG. 1. A MAC discretization cell in 3D.

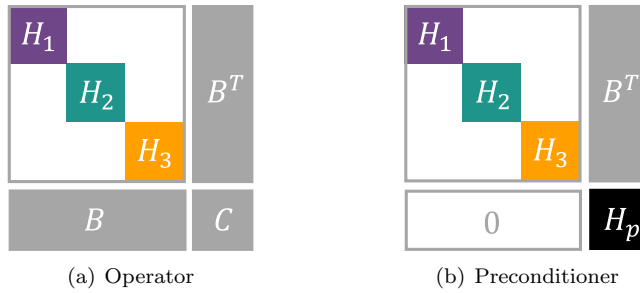


FIG. 2. On the left, the block structure of the discretized elastic Helmholtz equation in mixed formulation in 3D. On the right, the block structure of the block-acoustic preconditioner in 3D.

and \mathbf{u}_3 on different faces, and the pressure \mathbf{p} as well as the physical variables $\gamma, \rho, \lambda, \mu$ in the cell centers, see Figure 1.

The discretized system is given by

$$(2.6) \quad \begin{pmatrix} A & B^T \\ B & -C \end{pmatrix} \begin{pmatrix} \vec{\mathbf{u}} \\ \mathbf{p} \end{pmatrix} := \begin{pmatrix} \vec{\nabla}_h^T A_e(\boldsymbol{\mu}) \vec{\nabla}_h - \omega^2 M & \nabla_h \\ \nabla_h^T & \text{diag} \left(-\frac{1}{\lambda + \mu} \right) \end{pmatrix} \begin{pmatrix} \vec{\mathbf{u}} \\ \mathbf{p} \end{pmatrix} = \begin{pmatrix} -\vec{\mathbf{q}} \\ 0 \end{pmatrix}$$

where $A_e(\cdot)$ is an edge-averaging operator and $M = A_f(\boldsymbol{\rho}) \odot (1 - (\gamma/\omega)\iota)$ is a mass matrix, with $A_f(\cdot)$ being a face-averaging operator. A key feature of the resulting matrix, is that its main block is a block-diagonal matrix, comprised of three acoustic Helmholtz operators (in 3D). We utilize this block structure, depicted in Figure 2(a), in our preconditioning approach. I.e., the block-acoustic preconditioner that we present in the following section is a block-triangular matrix with acoustic Helmholtz operators on its diagonal, see Fig. 2(b).

2.2. Shifted Laplacian multigrid. The complex shifted Laplacian multigrid preconditioner (CSLP) [25] is a well known approach for the solution of the acoustic Helmholtz equation. Recently, an efficient adaptation for this method have been developed for the elastic Helmholtz equation [55]. Before presenting the two methods, we give general background on multigrid.

Multigrid methods [10] are a family of iterative solvers for linear systems of the form $H\mathbf{u} = \mathbf{q}$, that emerges from discretizations of PDEs. These methods are based on two complementary process: *smoothing*, or relaxation, to annihilate the high frequency modes of the error, and *coarse grid correction* to annihilate the remaining low frequency error modes. The former is done by applying an iterative method with

smoothing properties, and the latter is done by estimating and correcting the error \mathbf{e} , typically by solving a coarser analogue of the problem. The translation between the coarse and fine grids is done by intergrid operators called *restriction* R and *prolongation* P . Algorithm 2.1 summarizes the process using two grids. By treating the coarse problem recursively with one recursive call, we obtain the multigrid V-cycle, and by treating the coarse problem recursively with two recursive calls we obtain a W-cycle. For a more detailed description, see [12, 56].

Algorithm 2.1 Two-grid cycle.

Algorithm: $\mathbf{u} \leftarrow TwoGrid(H, \mathbf{q}, \mathbf{u})$.

1. Apply pre-relaxations: $\mathbf{u} \leftarrow Relax(H, \mathbf{u}, \mathbf{q})$
 2. Compute and restrict the residual $\mathbf{r}_c = P^T(\mathbf{q} - H\mathbf{u})$.
 3. Compute \mathbf{e}_c as the solution of the coarse-grid problem $H_c\mathbf{e}_c = \mathbf{r}_c$.
 4. Apply coarse grid correction: $\mathbf{u} \leftarrow \mathbf{u} + P\mathbf{e}_c$.
 5. Apply post-relaxations: $\mathbf{u} \leftarrow Relax(H, \mathbf{u}, \mathbf{q})$.
-

Standard multigrid methods are not effective in the solution of the acoustic Helmholtz equation (2.1). As observed in [21], the error amplification factor of a coarse grid correction, for a given eigenvector is given by

$$(2.7) \quad 1 - \frac{\lambda_h}{\lambda_H}$$

when λ_h is the eigenvalue corresponding to a given eigenvector on the fine grid, and λ_H is the eigenvalue corresponding to its coarsening. In indefinite systems, when exposed to many near-zero eigenvalues of different signs, the coarsened version of the same vector can lead to an eigenvalue of opposite sign, hence causing divergence of the method. An additional complex shift can make the expression in (2.7) smaller than one, and hence promise convergence of the multigrid method. The CSLP approach [25] is based on this observation. Let H be a matrix defined by a discretization of the Helmholtz operator. Define an attenuated operator

$$(2.8) \quad H_s = H - i\alpha\omega^2 M_s,$$

where M_s is some mass matrix, and $\alpha > 0$ is a shifting parameter. The shifted version can be solved by multigrid, and serves as a preconditioner for a discretized acoustic Helmholtz equation inside a suitable Krylov method such as (flexible) GMRES [50] or BiCGSTAB [59].

For the elastic Helmholtz equation, however, the shifted Laplacian preconditioner performs poorly, without additional adaptations. It was suggested in [55], to apply a zero-padded shift only on the leading block of the mixed formulation (2.5), rather than shifting the original formulation (2.3). Together with Vanka relaxation as a smoother, it resulted in an efficient monolithic multigrid preconditioner for the elastic Helmholtz equation. This preconditioner scales well with respect to the Poisson ratio, unlike previous multigrid methods for elastic Helmholtz. Yet, it does not scale with respect to the grid size, as the added shift depends on the frequency. This behavior is also evident in CSLP for the acoustic equation.

One of the major difficulties in the research of Helmholtz equation (acoustic or elastic) is achieving a wavenumber independent convergence, or, a scalability with respect to the grid size. High-frequency waves require fine meshes, at least 10 grid points per wavelength for standard second-order discretizations. To keep a constant

ratio of grid points per wavelength, the frequency ω increases in proportion to the grid size. It results in a larger shift in (2.8), for larger grids. Hence, one cannot expect a grid resolution independence whenever using a shift.

2.3. Approximate commutator preconditioners. An abundance of applications give rise to saddle-point systems, such as computational fluid dynamics, constrained optimization, finance, optimal control, and discretization of coupled PDE's, to name a few. Schur-complement preconditioning is a popular approach for saddle-point systems, see e.g. [20, 52]. A generalized saddle-point system and its block-triangular approximate Schur-complement preconditioner are typically given by

$$(2.9) \quad \mathcal{A} = \begin{pmatrix} A & B^T \\ B & -C \end{pmatrix}, \quad \mathcal{P} = \begin{pmatrix} A & B^T \\ 0 & \tilde{S} \end{pmatrix}$$

where \tilde{S} is an approximation of the Schur-complement $S = C + BA^{-1}B^T$. Forming and inverting the exact Schur-complement is *very costly* and during the past decades, there is an extensive search for cheap, yet reliable, approximations for its inverse.

Approximate commutator preconditioners form an important family of approximate Schur-complement preconditioners. The idea of approximate commutator preconditioning is based on utilizing the commutativity of the following differential operators in the continuous world²

$$(2.10) \quad \nabla \cdot \vec{\Delta} = \Delta \nabla \cdot,$$

to construct easy-to-invert approximations for the Schur-complement. In typical applications, B from Eq. (2.9) represents a discrete minus divergence operator, and A is a discrete minus vector Laplacian, with or without an added mass term or convective term. The continuous commutation relations (2.10) does not take into account the locations of the variables in a staggered discretization. To utilize similar commutation relations in the discrete space, one might look for an operator A_p , that mimics A but lives in the pressure's space, such that the commutator

$$(2.11) \quad \Xi = BA - A_p B$$

is small, in some sense.

Based on this notion, the F_p [20] or PCD [23] preconditioner was suggested, for standard Stokes-like systems with $C = 0$. In this approach, the Schur-complement is approximated by

$$(2.12) \quad BA^{-1}B^T \approx BD_u B^T A_p^{-1} D_p \quad \text{or} \quad BA^{-1}B^T \approx D_p A_p^{-1} B D_u B^T$$

where D_u and D_p are the lumped velocity and pressure mass matrices resulting from the finite element discretization, and A_p is a re-discretization of A on the pressure's space. Another well-studied approximate commutator approach for Stokes-like systems is the BFBt [20, 23] or LSC [18] preconditioning approach, giving the following approximation for the Schur-complement:

$$(2.13) \quad BA^{-1}B^T \approx (BD_u^{-1}B^T)(BD_u^{-1}AD_u^{-1}B^T)^{-1}(BD_u^{-1}B^T).$$

Many works have been done on BFBt-like preconditioners [16, 17, 37, 52]. Some where focused on the adjustment of the method to Stokes problems with variable viscosity.

²Note that for MAC discretization with constant coefficients and periodic boundary conditions, the commutation is exact in the discrete world, as observed in [11].

The weighted BFBt methods given in [47, 48], for instance, suggest replacing D_u in (2.13) by $\text{diag}(A)$ or by a scaling matrix with the square root of the the viscosity values, to deal with Stokes problems of variable viscosity.

3. Derivation and analysis of the preconditioner. The recent introduction of a mixed-formulation for the elastic Helmholtz equation (2.6) raises the need for new preconditioners. The resulting saddle-point system has a highly indefinite leading block, non-zero C -block and varying coefficients. To this end, we present an approximate commutator Schur-complement-free preconditioner, whose blocks are acoustic Helmholtz operators with shear and pressure wave velocities.

Inspired by the notion of distributive relaxation [11, 31, 22], we present our preconditioner as an approximation of a distributed operator. Applying a left distributor to the system (2.6) gives

$$(3.1) \quad \begin{pmatrix} I & 0 \\ B & -A_p \end{pmatrix} \begin{pmatrix} A & B^T \\ B & -C \end{pmatrix} \begin{pmatrix} \vec{\mathbf{e}}_{\bar{u}} \\ \mathbf{e}_p \end{pmatrix} = \begin{pmatrix} I & 0 \\ B & -A_p \end{pmatrix} \begin{pmatrix} \vec{\mathbf{r}}_{\bar{u}} \\ \mathbf{r}_p \end{pmatrix},$$

where A_p should be taken as an acoustic Helmholtz operator with shear wave velocity, discretized in the pressure's locations. That is in order for A_p to mimic A , which is a block-diagonal matrix with acoustic Helmholtz operators of shear wave velocity on its diagonal (discretized in the displacement's locations). We take

$$(3.2) \quad A_p := BB^T \boldsymbol{\mu} - \omega^2 M_p$$

as a discretization of an acoustic Helmholtz operator on the pressure's locations, with *shear* wave velocity, and with the mass matrix $M_p = \text{diag}(\boldsymbol{\rho}(1 - \gamma/\omega\nu))$. The distributed system is

$$(3.3) \quad \underbrace{\begin{pmatrix} A & B^T \\ \Xi & H_p \end{pmatrix}}_{\mathcal{K}} \begin{pmatrix} \vec{\mathbf{e}}_{\bar{u}} \\ \mathbf{e}_p \end{pmatrix} = \begin{pmatrix} \vec{\mathbf{r}}_{\bar{u}} \\ B\vec{\mathbf{r}}_{\bar{u}} - A_p \mathbf{r}_p \end{pmatrix}$$

where Ξ is the commutator, as in (2.11), and

$$(3.4) \quad H_p := BB^T + A_p C$$

is an acoustic Helmholtz operator with *pressure* wave velocity, discretized on the pressure's space. Our block-acoustic preconditioner is then given by

$$(3.5) \quad \mathcal{P} = \begin{pmatrix} A & B^T \\ 0 & H_p \end{pmatrix}.$$

Note that A is a block-diagonal matrix with acoustic Helmholtz operators of shear wave velocity on its diagonal. Recall that the pressure wave velocity is typically lower than shear wave velocity, making H_p is easier to solve iteratively compared to the diagonal block comprising A . The block structure of \mathcal{P} , comprised of acoustic Helmholtz diagonal blocks discretized in different locations, is depicted in Fig. 2(b). This structure enables the solution of three (in 2D) or four (in 3D) acoustic problems instead of one elastic Helmholtz problem.

REMARK 3.1 (Choice of A_p). *In (3.2), we chose to put the weighting $\boldsymbol{\mu}$ to multiply the Laplacian from the right. One might consider taking $\tilde{A}_p = BA_f(\boldsymbol{\mu})B^T - \omega^2 M_p$ instead of A_p , placing the weighting between the minus divergence and the gradient,*

which better resembles the blocks of A , according to (2.6). Nevertheless, our aim is to reduce the commutator Ξ in (2.11). Specifically, using A_p , the dominant part of our commutator (neglecting mass terms) ends up being

$$(3.6) \quad B((\nabla \cdot)_h A_e(\boldsymbol{\mu}) \nabla_h) - BB^T \boldsymbol{\mu} B,$$

while using \tilde{A}_p , the corresponding part of the commutator would have been

$$(3.7) \quad B((\nabla \cdot)_h A_e(\boldsymbol{\mu}) \nabla_h) - BA_f(\boldsymbol{\mu}) B^T B.$$

In (3.6), a derivative operator is applied on $\boldsymbol{\mu}$ twice from the left in both summands. On the other hand, in (3.7), the right term has only one derivative applied on $\boldsymbol{\mu}$ from the left. For smooth media, \tilde{A}_p and A_p yields equivalent methods. Yet, we see in practice a significant gain for choosing A_p for non-smooth media.

3.1. A sufficient condition for convergence. The commutator has a crucial role in the designing of approximate commutator preconditioners. However, as Elman, Silvester and Wathen noticed in their book [22], Remark 9.5, approximate commutator preconditioners can sometimes be effective even when the commutator is not small in norm. The theorem below explains why the commutator alone does not suffice to predict convergence of our preconditioner, and suggests a more reliable measure.

THEOREM 3.1. *Let \mathcal{K} be the distributed matrix from (3.3) and let \mathcal{P} be the preconditioner from (3.5). Denote by n the size of A and by m the size of A_p from (3.2). Then the preconditioned matrix $\mathcal{P}^{-1}\mathcal{K}$ has an eigenvalue $\lambda = 1$ with multiplicity of at least n . Namely, the corresponding error iteration matrix $T = I - \mathcal{P}^{-1}\mathcal{K}$ has a nullspace of dimension at least n .*

Moreover, Let Z be the $m \times m$ matrix

$$(3.8) \quad Z = \Xi A^{-1} B^T H_p^{-1}.$$

Then

$$(3.9) \quad \text{spec}(T) = \text{spec}(Z) \cup \{0\},$$

and consequently, $\rho(T) = \rho(Z)$.

Proof. We first prove that the multiplicity of the eigenvalue 1 in the preconditioned system is at least n . A straightforward calculation shows

$$(3.10) \quad \mathcal{P}^{-1}\mathcal{K} = \begin{pmatrix} A^{-1} & -A^{-1}B^T H_p^{-1} \\ 0 & H_p^{-1} \end{pmatrix} \begin{pmatrix} A & B^T \\ \Xi & H_p \end{pmatrix} = \begin{pmatrix} I_n - A^{-1}B^T H_p^{-1} \Xi & 0 \\ H_p^{-1} \Xi & I_m \end{pmatrix}.$$

Therefore, it is readily seen that $\mathcal{P}^{-1}\mathcal{K}$ has at an eigenvalue 1 with multiplicity of at least m . Furthermore, the $n \times n$ matrix

$$(3.11) \quad Y = A^{-1} B^T H_p^{-1} \Xi$$

is rank-deficient, with

$$(3.12) \quad \text{rank}(Y) \leq \text{rank}(B^T) \leq m.$$

Hence, Y has a nullspace of at least $n - m$ dimensions, and consequently, $I - Y$ has the eigenvalue 1 with a multiplicity of at least $n - m$. Overall, the multiplicity of the eigenvalue 1 in $\mathcal{P}^{-1}\mathcal{K}$ is at least n .

Second, we prove that

$$(3.13) \quad \text{spec}(T) = \text{spec}(Y).$$

A straightforward calculation gives

$$(3.14) \quad T = I - \mathcal{P}^{-1}\mathcal{K} = \begin{pmatrix} Y & 0 \\ -H_p^{-1}\Xi & 0 \end{pmatrix}.$$

Evidently, the eigenvalues of T are those of Y and zero. Since Y is a rank deficient matrix, it is therefore clear that the spectrums of Y and T are equal.

Finally, we prove that

$$(3.15) \quad \text{spec}(Y) \setminus \{0\} = \text{spec}(Z) \setminus \{0\}.$$

Indeed, let (λ, \mathbf{v}) be an eigenpair of Y with $\lambda \neq 0$. Denote $\mathbf{w} = \Xi\mathbf{v}$. Then,

$$(3.16) \quad Y\mathbf{v} = A^{-1}B^T H_p^{-1}\mathbf{w} = \lambda\mathbf{v} \quad \Rightarrow \quad \Xi Y\mathbf{v} = Z\mathbf{w} = \lambda\mathbf{w}.$$

Notice that \mathbf{w} is a nonzero vector (otherwise λ would be zero). Hence, (λ, \mathbf{w}) is an eigenpair of Z , and thus $\text{spec}(Y) \setminus \{0\} \subseteq \text{spec}(Z) \setminus \{0\}$. The inclusion in the other direction \supseteq is achieved similarly, by multiplying $Z\mathbf{v} = \lambda\mathbf{v}$ from the left by $A^{-1}B^T H_p^{-1}$. Consequently, the spectrum of the error iteration matrix is $\text{spec}(Z) \cup \{0\}$. \square

As an immediate consequence of Theorem 3.1, a splitting method in which the splitting operator is the preconditioner, converges if and only if $\rho(Z) < 1$. Moreover, $\rho(Z)$ gives an upper bound for the asymptotic convergence rate of such a splitting method. Clearly, the convergence of the splitting method implies the convergence of the corresponding preconditioned Krylov method, and hence $\rho(Z) < 1$ is a sufficient condition for convergence of our method. Yet, the preconditioned Krylov method might converge rapidly even when $\rho(Z) > 1$ and the rate also depends on the scattering of the eigenvalues. To simplify the discussion below, we refer to $\rho(Z)$ as a measure for convergence, even though our method is implemented as a preconditioned Krylov iteration.

Theorem 3.1 sheds light on the role of the commutator in determining the convergence. It was noticed long ago that convergence of approximate commutator preconditioners might occur even when the commutator is large in norm, and we show later in Section 4 that two problems with almost the same commutator might differ in convergence rates. This interesting phenomenon appears here when taking the same media but different frequencies or attenuations. It can be explained by splitting the commutator to a Laplacian-related part and a mass-related part:

$$(3.17) \quad \Xi = \underbrace{B(\vec{\nabla} \cdot A_e(\boldsymbol{\mu})\vec{\nabla}) - (BB^T \boldsymbol{\mu})B}_{\Xi_{lap}} - \underbrace{\omega^2(1 - (\gamma/\omega)\iota)BA_f(\boldsymbol{\rho}) - \text{diag}(\boldsymbol{\rho})B}_{\Xi_{mass}}.$$

Typically we observe that $\Xi_{mass} \ll \Xi_{lap}$, because we have only first derivatives in Ξ_{mass} (represented by B) compared to higher-order derivatives in Ξ_{lap} . Evidently, the commutator is not sensitive to changes in frequency and attenuation that comprises the mass term, but the convergence deteriorates as the frequency grows and improves as the attenuation grows. Hence, the commutator norm alone cannot determine the convergence in this case.

Now, Theorem 3.1 suggests the spectrum of Z from Eq. (3.8) as a better measure for convergence. In particular, it manages to encapsulate the influence of the

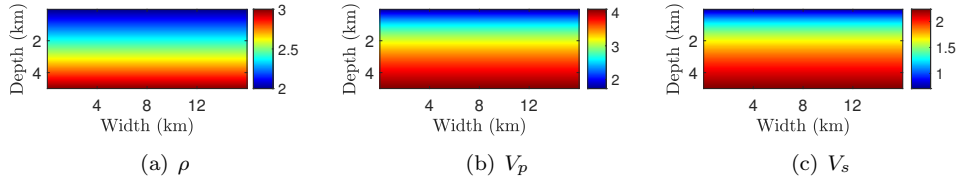


FIG. 3. *The elastic linear model. Velocity units: km/sec, density units: g/cm³.*

frequency and attenuation, which the commutator fails to detect. Even a small commutator — multiplied by the inverse of A and of H_p — might lead to a significantly larger $\rho(Z)$, if any of these matrices has near zero eigenvalues. It occurs, for instance, for high frequency and low attenuation problems. For smooth media, the commutator is typically so small, so we overcome this difficulty. However, in highly heterogeneous high frequency problems, an additional shift, physically representing an added artificial attenuation, might be necessary for the block-acoustic preconditioner to converge (similarly to its necessity in the context of shifted Laplacian multigrid). The additional attenuation shifts the eigenvalues of A and in H_p in the complex plane, hence preventing near zero eigenvalues. Nevertheless, we still want to solve the original problem, and the shifted problem acts only as an aid, so a large shift can hamper the convergence and interfere with the scalability.

To summarize, although it was long ago stated that the commutator does not determine the convergence, to the best of our knowledge, no alternative measure was suggested prior to Theorem 3.1 above. We note that forming Z is expensive computationally and requires the inversion of A and H_p , hence it should not be seen as a predictive tool, rather as an analytical one, which explains the convergence patterns we see in practice. Furthermore, although Theorem 3.1 is formulated for the specific case of our block-acoustic preconditioner, it gives rise to similar results for other approximate commutator preconditioners, which we leave for future investigation.

4. Numerical results. In this section we perform numerical experiments to establish the efficiency and robustness of our method. In Subsection 4.1 we demonstrate scalability properties of our preconditioner, and in Subsection 4.2 we verify the theoretical result of Theorem 3.1 and its implications. In Subsection 4.3 we compare our block-acoustic preconditioner to other approximate commutator preconditioners, and discuss the limitations of this comparison. In Subsection 4.4, we show the superiority of our preconditioner — with a shifted Laplacian multigrid solve of each block — over the monolithic multigrid method suggested in [55]. Finally, in Subsection 4.5 we demonstrate the effectiveness of our preconditioner in solving real-world 3D problems with challenging geophysical media.

Throughout the experiments, we solve the discretized elastic Helmholtz problem in mixed formulation (2.6) on a finite rectangular domain (or cubic, in 3D), subject to a point-source located in the center of the top edge (or face) of the domain, up to a tolerance of relative residual $< 10^{-6}$. The ABC are implemented as a layer of gradually increasing attenuation γ , of width of 20 grid cells. This is additional to a basic natural attenuation of $\gamma = 0.01\pi$ that we assume throughout the domain, in all of our experiments. The default frequency corresponds to at least 10 grid points per shear wavelength. That is, in heterogeneous media and unless specified otherwise, the most challenging region has about 10 grid points per shear wavelength.

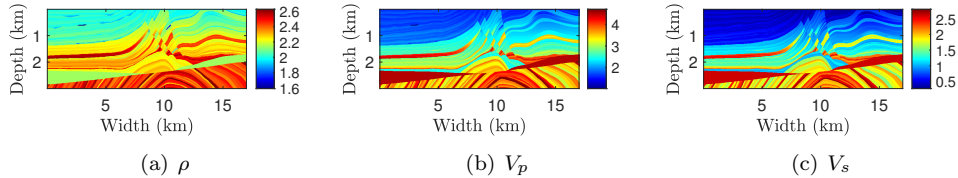


FIG. 4. *The elastic Marmousi2 2D model. Velocity units: km/sec, density units: g/cm³.*

Our code is written in the `Julia` language [8], and is included as a part of the `jInv.jl` package [49]. This package enables using of our code as a forward solver for elastic full waveform inversion in the frequency domain. Our tests were computed on a simple dual-core laptop with 32 GB RAM, running Windows 10.

For the 2D experiments in the next three subsections, we use the following models:

- **Homogeneous media:** a dimensionless domain $\Omega = [0, 16] \times [0, 5]$, with constant ρ , λ and μ . Our default values are $\rho = \mu = 1$ and $\lambda = 16$, which corresponds to Poisson ratio $\sigma = 0.47$. As noted before, in our discretization, the commutation is exact for this media in the interior of the domain. However, due to the application of ABC, the coefficient γ non-constant, even for constant media.
- **Linear media:** a domain of width 16 km and depth 5 km, with density and Lamé coefficients that varies linearly in the vertical dimension. Our default ranges are $\rho \in [2, 3]$, $\mu \in [1, 15]$ and $\lambda \in [4, 20]$, which corresponds to Poisson ratio of at most $\sigma = 0.4$. Figure 3 shows the density and wave velocities.
- **Marmousi2 media:** an elastic 2D geophysical model suggested in [40], based on a section of the Kwanza basin in Angola. The domain is very shallow: 17 km width and only 3 km depth, so we add a vertical extension of 16 cells in the bottom, to facilitate the application of the ABC. Figure 4 shows the (non-extended) model.

4.1. Scalability. In the first experiment, we show the scalability properties of our preconditioner. Table 1 counts the non-restarted GMRES iterations needed to solve the linear model problem for different grid sizes. We repeat the experiment for three more variants of the default linear model, in which the λ range is multiplied by 10, 100 and 1000. The aim of this modification is enlarging the Poisson ratio while retaining the smoothness of the media. The iteration count does not exceed 19, for any of the grid sizes and Poisson ratios examined. That is, the method is scalable with respect to the Poisson ratio and with respect to the grid size.

The latter is analogous to a property sought in many works regarding the acoustic Helmholtz equation: *wavenumber independent convergence*. Table 1 shows a nearly constant iteration count, regardless of the frequency, which is chosen for each grid size to keep a ratio of about 10 grid points per shear wavelength in the most challenging regime of the domain. However, in large real-world instances, it is impractical to solve each block directly as we do here, and most existing iterative solvers for acoustic Helmholtz require a shift — which interferes with the scalability with respect to the grid size. Yet, the results above gives rise to future investigation of the acoustic Helmholtz equation: once an acoustic scalable solver will be developed, it will be automatically applicable for the elastic case via our preconditioner, without harming the scaling properties.

Non-restarted GMRES iteration count, linear media				
Grid size (cells)	$\lambda \cdot 1$	$\lambda \cdot 10$	$\lambda \cdot 100$	$\lambda \cdot 1000$
200×64	14	13	13	13
400×128	14	13	12	12
800×256	14	16	12	11
1600×512	14	19	12	12

TABLE 1

Number of block-acoustic preconditioning cycles needed for convergence for the 2D elastic Helmholtz equation in linear media. Each acoustic block is solved directly. Linear media with different Poisson ratios were implemented by a point-wise multiplication of λ by different factors. The highest factor applied on λ corresponds to a Poisson's ratio $\sigma \geq 0.4996$ all over the grid.

4.2. Demonstration of Theorem 3.1. In this subsection we verify numerically the result from Theorem 3.1 and study its implications. Recall that Z , defined in (3.8), is an $n_{cells} \times n_{cells}$ matrix that — as proved in Theorem 3.1 — captures all the spectral information on the error iteration matrix T .

In Figure 5 we depict the spectrum of Z for different media and different frequencies, represented as different numbers of grid points per shear wavelength, G_s . Since forming Z and calculating its entire set of eigenvalues is very costly, we hold this experiment for a small 50×50 cells slice of the homogeneous media, of the linear media (of original size 128×64 cells) and of Marmousi2 media (of original size 544×112 cells). We stress that this slicing causes loss of some of the heterogeneity encapsulated by the media, therefore, we draw only qualitative conclusions from the comparison. We observe that the spectrum becomes more scattered as the heterogeneity and non-smoothness grows. Moreover, we observe that when a higher frequency is taken for the same media, some eigenvalues scatter far away from zero. As expected from the discussion in Subsection 3.1, the near zero eigenvalues of the highly indefinite A causes this phenomenon, that can be relaxed by an additional shift.

Figure 6 shows the spectral radius of Z for linear media of size 400×128 and Marmousi2 media of size 544×112 as a function of the shift. We implemented this by applying the power method on a mat-vec code of Z , without forming the matrix. We observe that increasing the shift lowers the spectral radius, as expected. For linear media of the given size, the minimal shift needed to for the spectral radius to be lower than 1, is negligible, as it is in the same order of magnitude as the natural attenuation that we use in our experiments. For Marmousi2 media of the given size, a larger shift of about 0.1 is required for the spectral radius to be lower than 1.

4.3. Comparison with other approximate commutator methods. In this subsection we compare the block-acoustic preconditioner to existing preconditioners described in Subsection 2.3. Nevertheless, the latter were developed for incompressible fluid flow problems, and are described in terms of finite elements discretization. We apply a naive implementation of F_p from (2.12)³ and BFBt from (2.13), replacing the finite elements mass matrices by identity matrices, and the convection-diffusion leading block by our A from (2.6).

Needless to say, the comparison of methods that were developed for such different problems is not quite equitable. There are two main differences between the

³We took the left equation of (2.12), but observed that the other version behaves similarly in all of our experiments.

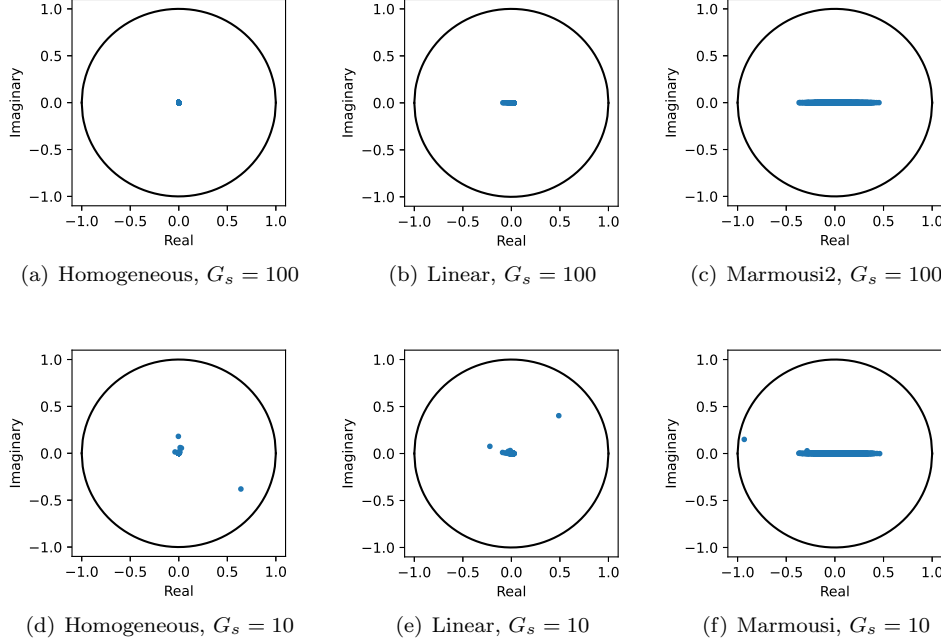


FIG. 5. The spectrum of Z from (3.8) for a 50×50 cells slice of different media and frequencies.

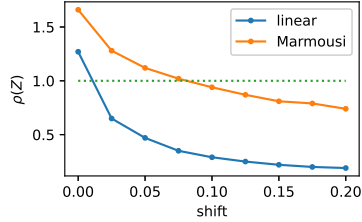


FIG. 6. the spectral radius of Z from (3.8) for linear media of size 400×128 cells and Marmousi2 media of size 544×112 cells (before the vertical extension), as a function of the shift.

Stokes-like systems and elastic Helmholtz saddle-point system: the indefiniteness of the leading block, and the existence of a non-zero C block. We suggest two adaptations, to accommodate for the differences: testing the performance for a wide range of frequencies, including $\omega \approx 0$ for which the leading block is SPD, and testing different Poisson ratios, including a nearly incompressible case.

In the first experiment, we apply the block-acoustic, F_p and BFBt preconditioners to a model problem of homogeneous media with a grid size of 128×64 cells, for various values of ω . Figure 7 shows the GMRES(5) iteration count as a function of the frequency. The smallest ω that we take is negligible (corresponds to 10^4 grid points per shear wavelength), and resembles a linear elasticity problem. The largest ω corresponds to about 11 grid points per wavelength. For the linear elasticity problem, the preconditioners function similarly, whereas for high-frequency elastic Helmholtz, the block-acoustic preconditioner outperforms the other examined approximate com-

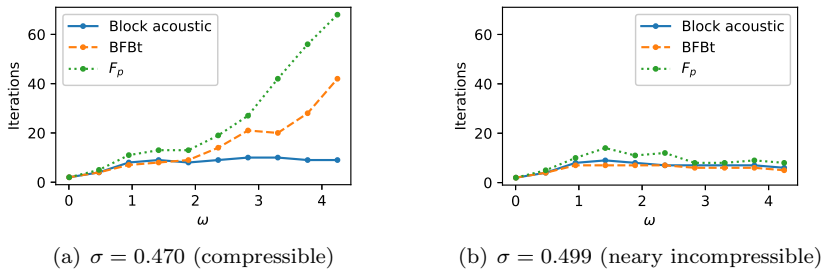


FIG. 7. Number of preconditioned GMRES(5) iterations needed for convergence for the elastic Helmholtz equation in constant media, as a function of the frequency. The lowest frequency is negligible and corresponds to about 100 grid points per shear wavelength, and the highest frequency corresponds to about 11 grid points per shear wavelength. On the left, the default constant media was taken, and on the right, it was altered by multiplying the lamé coefficient λ by 1000.

mutator preconditioners. In the second experiment, we repeat the first experiment for nearly incompressible media. That is, an identical shear wave velocity and a higher Poisson ratio. In Figure 7 we see that the three preconditioners solve the problem by a similar rate in the nearly incompressible case. This result is somewhat surprising and requires further investigation, as the F_p and $BFBt$ preconditioners were *not* originally designed for saddle-point systems with an indefinite leading block, and to the best of our knowledge, were not investigated in this context previously.

To sum up, in linear elasticity problems, low frequency problems (of about 20 grid points per shear wavelength or more) and in the nearly incompressible case — the methods preform similarly. Though, the aim of the elastic Helmholtz equation is modeling waves in *solids*, which are compressible. Incompressible elastic Helmholtz is in fact reducible to acoustic Helmholtz, as shown in Subsection 2.1. Moreover, we performed the above mentioned comparison on homogeneous media only, since the methods from Subsection 2.3, in our implementation, preformed poorly for linear and Marmousi2 media.

4.4. Monolithic vs. block-preconditioned multigrid. In this section we compare the performance of the block-acoustic multigrid preconditioner — our preconditioner combined with CSLP solve of each acoustic block — to the monolithic multigrid preconditioner from [55], described in Subsection 2.2. We first present the multigrid setup of the two methods, followed by a FLOP calculation for each. Finally, we show the iteration count and total computational cost for different media.

4.4.1. Multigrid setup. First, we describe the multigrid setup for the block-acoustic multigrid preconditioning. In each preconditioning step, we approximately solve each block of the block-acoustic preconditioner by a $W(1, 2)$ cycle of CSLP [25], with damped Jacobi as a smoother. The damping parameters on the first, second and third levels are 0.8, 0.8 and 0.3.

We use different intergrid operators for each diagonal block, corresponding to the location on the staggered grid. The diagonal blocks in (3.5) (in 2D) are A_1 , discretized on the \mathbf{u}_1 faces, A_2 on the \mathbf{u}_2 faces, and H_p which is cell centered. For each of them, we take the restriction to be a Kroncker product of the 1D restrictions defined by the stencil $\begin{bmatrix} 1 & 2 & 1 \end{bmatrix}$ for the nodal direction and by the stencil $\begin{bmatrix} 1 & 3 & * & 3 & 1 \end{bmatrix}$ for the cell-centered direction. For instance, \mathbf{u}_1 is nodal in the x direction and cell-centered

in the y direction and hence

$$(4.1) \quad R_{u_1} = \frac{1}{4} [1 \quad 2 \quad 1] \otimes \frac{1}{8} [1 \quad 3 \quad * \quad 3 \quad 1]$$

is the restriction for the block A_1 . The restriction R_{u_2} is defined similarly. The restriction for H_p is

$$(4.2) \quad R_p = \frac{1}{8} [1 \quad 3 \quad * \quad 3 \quad 1] \otimes \frac{1}{8} [1 \quad 3 \quad * \quad 3 \quad 1].$$

The prolongations are defined as $P_{u_1} = 2R_{u_1}^T$ and similarly for P_{u_2} and P_p .

The coarse grid operator is determined by Galerkin coarsening. That is, e.g.,

$$(4.3) \quad (H_p)_H = R_p(H_p)_h P_p.$$

The coarsest grid problem is solved directly using LU decomposition.

For the monolithic multigrid, we use Vanka red-black smoother with relaxation parameters of 0.65, 0.5 and 0.3 for the first, second and third grid, respectively. We use $W(1,1)$ cycles with Galerkin coarsening and solve the coarsest grid directly. As intergrid operators, we take a mixed version: the prolongation is

$$(4.4) \quad P = \text{blockdiag}(P_{u_1}, P_{u_2}, P_p)$$

where P_{u_1}, P_{u_2} and P_p are as in the block-acoustic case. However, the restriction is *not* a scaled transpose of the prolongation: we take $R = \text{blockdiag}(\tilde{R}_{u_1}, \tilde{R}_{u_2}, \tilde{R}_p)$ where

$$(4.5) \quad \tilde{R}_{u_1} = \frac{1}{4} [1 \quad 2 \quad 1] \otimes \frac{1}{2} [1 \quad * \quad 1] \text{ and } \tilde{R}_p = \frac{1}{2} [1 \quad * \quad 1] \otimes \frac{1}{2} [1 \quad * \quad 1]$$

and \tilde{R}_{u_2} is defined similarly to \tilde{R}_{u_1} .

The choice of mixed intergrid in the monolithic case reduces the complexity of the operators, while keeping almost the same convergence rate, as mentioned in [55, 63]. For the block-acoustic case in 2D, however, we have seen by trial and error that the mixed intergrid is less favorable. The different number of relaxation cycles in the $W(1,2)$ Jacobi compared to $W(1,1)$ Vanka, compensates for the additional computational cost. In fact, Vanka relaxation has about twice the computational cost of Jacobi relaxation (as calculated in the next subsection), but taking more than 3 relaxations per cycle did not lead to any additional improvement in convergence of the block-acoustic multigrid.

4.4.2. FLOP count. Since the comparison of the two different multigrid frameworks is not equitable, we first include a detailed FLOP count for each of the methods. The results are displayed in Table 2, including the sum of two FLOP sources: the analytically estimated computational cost for the entire preconditioning step except for the coarse solve, and the number of non zeros in the resulting LU decomposition. Below, we demonstrate the analytic estimation, not including the coarsest solve, for the case of a two-level cycle.

We count the costs of residual, relaxation and intergrid calculation for each method. For the block-acoustic method, we add the cost of forming the corrected right-hand-side in (3.3). We estimate the FLOPs by counting number of nonzeros. Denoting the number of cells by n_{cells} , we neglect terms of order $\sqrt{n_{cells}}$.

FLOP count per cell						
	Block-acoustic multigrid			Monolithic multigrid		
Grid size	2-level	3-level	4-level	2-level	3-level	4-level
400×128	193	261	332	349	355	486
800×256	223	274	340	446	396	501
1600×512	277	291	346	558	445	522

TABLE 2

The total FLOP count per cycle per discretization cell, including the number of nonzeros of the LU factors. In the block acoustic case, for three $W(1,2)$ cycles with Jacobi relaxation for the blocks A_1 , A_2 and H_p . In the monolithic case, for a $W(1,1)$ cycle with Vanka relaxation.

In each block-acoustic multigrid preconditioning step, in 2D, three $W(1,2)$ cycles are applied, one for each of the 5-diagonal matrices A_1 , A_2 and H_p of size $n_{cells} \times n_{cells}$. The residual calculation costs $15n_{cells}$. A Jacobi step includes residual calculation and an additional $1n_{cells}$, resulting in $54n_{cells}$. The restriction R_{u_1} from (4.1) and R_{u_2} has 12 nonzeros per row, and the restriction R_p from (4.2) has 16 nonzeros per row, leading to a total cost of $20n_{cells}$ for intergrid operations. The calculation of the corrected right-hand-side in (3.3) costs $9n_{cells}$, because A_p is 5-diagonal and B is a concatenation of two 2-diagonal matrices. To sum up, excluding the LU solve in the coarse grid, one preconditioning cycle costs $98n_{cells}$ FLOPs.

For the monolithic multigrid, the residual computation sums up to $19n_{cells}$ nonzeros (counting the diagonals of all blocks in (2.6)). One Vanka relaxation includes a residual calculation and additional $17n_{cells}$ FLOPs, when the special structure of the 5×5 submatrices is exploited, as noted in [63], Remark 3.1. The total relaxation cost for a $W(1,1)$ cycle is thus $72n_{cells}$. The prolongation cost is identical to the block-acoustic case, and the restriction is slightly cheaper: \tilde{R}_{u_1} and \tilde{R}_p from (4.5) has 6 and 4 nonzeros per row, respectively, each having $0.25n_{cells}$ rows. Hence, the total intergrid cost is $14n_{cells}$. It sums up to $105n_{cells}$ per cycle, excluding the LU cost.

A major part of the total computational cost is invested in the coarse grid solve. In 2D, the coarse grid LU factors of the monolithic multigrid 2.5 times heavier than the three pairs of factors in the block-acoustic multigrid altogether. It can be explained by the coupling of the multi-diagonal blocks in the elastic Helmholtz operator in mixed formulation (2.6). This coupling, together with the Galerkin coarsening, leads to rather dense LU factors. In 3D, the fill-in is more severe: we observed a 5 times heavier coarse solve for monolithic method, compared to the block-acoustic, for two-level method applied on a toy-size grid of $64 \times 64 \times 32$ cells. Since the fill-in is characterized by super-linear growth, for large 3D grids the LU decomposition constitutes the majority of the overall cost, making the advantage of the block-acoustic approach even bigger.

4.4.3. Iteration count and computational cost. Tables 3 and 4 shows the iteration count of the block-acoustic multigrid vs. monolithic multigrid. The shift for each experiment was chosen by trial and error, to optimize the convergence. The total computational cost (given in parentheses) is computed by multiplying the iteration number by the corresponding number from Table 2 and normalizing⁴.

⁴For brevity, Table 2 includes only the grid sizes used for the linear model. For other media, we use similarly calculated values that we do not present here.

GMRES(5) iteration count for linear media						
Grid size	Block-acoustic multigrid			Monolithic multigrid		
	2-level $\alpha = 0.1$	3-level $\alpha = 0.2$	4-level $\alpha = 0.4$	2-level $\alpha = 0.1$	3-level $\alpha = 0.4$	4-level $\alpha = 0.5$
400×128	31 (0.6)	49 (1.3)	90 (3)	31 (1.1)	79 (2.8)	98 (4.8)
800×256	49 (1.1)	93 (2.5)	171 (5.8)	67 (3)	171 (6.8)	216 (10.8)
1600×512	86 (2.4)	204 (6)	361 (12.5)	161 (9)	414 (18.4)	519 (27.1)

TABLE 3

Number of preconditioning cycles needed for convergence with the monolithic or block-acoustic multigrid, for the 2D elastic Helmholtz equation in linear media. In the monolithic preconditioner, a red-black cell-wise Vanka smoother is used for a $W(1,1)$ cycle, and in the block-acoustic multigrid, a damped Jacobi smoother is used for a $W(1,2)$ cycle. In parentheses, ten-thousands of n_{cells} FLOPs.

GMRES(5) iteration count for Marmousi2 media						
Grid size	Block-acoustic multigrid			Monolithic multigrid		
	2-level $\alpha = 0.2$	3-level $\alpha = 0.2$	4-level $\alpha = 0.5$	2-level $\alpha = 0.1$	3-level $\alpha = 0.2$	4-level $\alpha = 0.6$
544×128	78 (1.5)	78 (2)	143 (4.7)	30 (1)	54 (1.9)	157 (7.6)
1088×240	146 (3.2)	143 (3.9)	305 (10.3)	65 (2.8)	124 (4.8)	334 (16.7)
2176×464	445 (12.1)	444 (12.9)	662 (23)	140 (7.3)	408 (17.6)	703 (36.5)

TABLE 4

Number of preconditioning cycles needed for convergence with the monolithic or block-acoustic multigrid, for the 2D elastic Helmholtz equation in Marmousi2 media. In the monolithic preconditioner, a red-black cell-wise Vanka smoother is used for a $W(1,1)$ cycle, and in the block-acoustic multigrid, a damped Jacobi smoother is used for a $W(1,2)$ cycle. In parentheses, ten-thousands of n_{cells} FLOPs.

Table 3 includes the GMRES(5) iteration count and total computational cost for linear media. The block-acoustic multigrid achieves a significantly smaller iteration count for 3-level, 4-level and for the larger grids with 2-level. Taking into account the cost per iteration, the block-acoustic multigrid preconditioner accelerates the solution by a factor of 2 and more.

As explained in Subsection 2.2, full scalability with respect to the grid size cannot be expected for any shifted method. However, the block-acoustic multigrid yields significantly improved scaling: the average growth in iterations for the block-acoustic approach varies from $\times 1.7$ for the 2-level method to $\times 2$ for the 4-level method, while for the monolithic approach the growth factor is about $\times 2.3$, regardless of the levels. The reason for this improved scalability is not fully clear. It might occur since on larger grids, the linear media looks smoother, leading to a smaller commutator and a smaller spectral radius of the matrix Z from Theorem 3.1.

Table 4 shows the GMRES(5) iteration count and total computational cost for Marmousi2 media. The iteration count for the 2-level method is significantly higher for the block-acoustic method, which can be explained by the larger shift required for the method. For 3-level and 4-level methods, the iteration count is comparable between the two methods. The iteration growth factor is quite similar for the two method, and varies between $\times 2.1$ to $\times 2.8$ for different number of levels. Taking

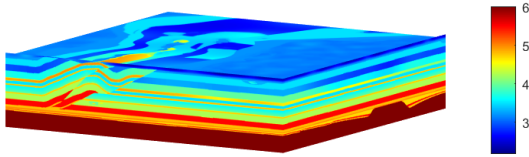


FIG. 8. *The Overthrust model. Velocity units: km/sec.*

into account the cost per iteration, the block-acoustic achieves a considerably lower computational cost, without worsening the scaling.

4.5. Three-dimensional experiments. In this subsection we demonstrate the applicability of our preconditioner, combined with a multigrid solve of each block, to 3D problems. We perform the experiments on the Overthrust model [1], a geophysical 3D model with jumping coefficients. This is an acoustic model, and its pressure wave velocity is depicted in Figure 8. We define the shear wave velocity as $V_s = 0.5V_p$ and the density as $\rho = 0.25V_p + 1.2$ to modify it to represent elastic media. The model is shallow, and extended similarly to Marmousi2.

The multigrid framework is similar to Subsection 4.4, with two modifications: First, we use mixed intergrid as in (4.5). Second, we take Jacobi $W(2, 2)$ cycles with damping parameters of 0.8, 0.8 and 0.2 for the first, second and third level respectively. These modifications, as we observed by trial and error, improve convergence of the method for the 3D case.

The results are included in Table 5, demonstrating that the block-acoustic preconditioner enables the solution of the 3D elastic Helmholtz equation in the Overthrust medium with a small number of iterations. Moreover, the memory consumption is notably low: we manage to solve here a problem with about 46 million unknowns using a laptop with 32 GB memory only. For the sake of comparison, in [55] and in [63] the largest systems to be solved by a 256 GB workstation had about 70 million unknowns, although the LU factors of the coarse grid were *not* computed and saved in any of these works. A domain decomposition coarse grid solver had been applied in [55], and the coarse grid in [63] was solved iteratively with hybrid Kaczmarz relaxation as a preconditioner.

In this work, we solve large 3D problems without any special adaptation to deal with the coarse grid. The decoupled block structures enables, besides the improved sparsity of the LU factors, an additional advantage thanks to the natural parallelization. Since each of the blocks can be solved separately, one can save the 4 pairs of LU factors to the disc, extracting them only when needed, thus reducing by a factor of 4 the total RAM memory consumption of the coarse grid solve. The grid sizes in Table 5 were achieved without utilizing disc memory.

5. Conclusion. In this work we introduced a block-acoustic preconditioner for the elastic Helmholtz equation. Building upon the commutation of the underlying operators in the continuous space, our key idea is designing an approximation of the leading block discretized in the pressure's space that will enable a small enough commutator. It results in a block-triangular preconditioner whose diagonal blocks are acoustic Helmholtz operators. Our theoretical results unravel the role of the commutator in the preconditioning of systems with an indefinite leading block. We demonstrated both analytically and numerically that a complex shift might be necessary, in highly heterogeneous media, to promise fast convergence. However, without a

Iteration count for 3D Overthrust media			
Grid size	2-level	3-level	4-level
	$\alpha = 0.1$	$\alpha = 0.2$	$\alpha = 0.4$
$128 \times 128 \times 56$	24	22	32
$192 \times 192 \times 72$	29	29	49
$256 \times 256 \times 96$	oom	38	69
$320 \times 320 \times 112$	oom	43	98

TABLE 5

Number of block-acoustic preconditioned *GMRES*(5) iterations needed for convergence with block-acoustic multigrid, for the 3D elastic Helmholtz equation in Overthrust media. In each preconditioning step, one $W(2,2)$ cycle with mixed intergrid is applied with damped Jacobi relaxation. The abbreviation “oom” stands for an out of memory error on a 32 GB RAM laptop.

complex shift, the block-acoustic preconditioner is scalable with respect to the Poisson ratio and the grid size.

We designed an efficient combination of our preconditioner with shifted Laplacian multigrid applied on each acoustic block, and compared the method to a recent monolithic multigrid preconditioner. The resulting block-acoustic multigrid achieves significantly lower computational cost for smooth media. For challenging geophysical media with jumping coefficients, our approach attains comparable iteration count, yet lower computational cost, compared to the monolithic multigrid. The block structure of our preconditioner enables a huge memory save, in addition to the natural parallelization. Overall, the block-acoustic preconditioner makes the problem of elastic wave propagation in large 3D cases applicable on a laptop.

Acknowledgements. The authors are grateful to Prof. Howard Elman for inspiring discussions, for his careful reading of the manuscript, and for helpful comments and pointers to the literature.

REFERENCES

- [1] F. AMINZADEH, P. WEIMER, AND T. DAVIS, *3-d salt and overthrust seismic models*, *Studies in Geology*, 42 (1996), pp. 247–256.
- [2] O. AXELSSON AND M. NEYTICHEVA, *Eigenvalue estimates for preconditioned saddle point matrices*, *Numerical Linear Algebra with Applications*, 13 (2006), pp. 339–360.
- [3] Y. AZULAY AND E. TREISTER, *Multigrid-augmented deep learning preconditioners for the helmholtz equation*, *SIAM Journal on Scientific Computing*, (2022).
- [4] M. BAUMANN, R. ASTUDILLO, Y. QIU, E. Y. ANG, M. VAN GIJZEN, AND R.-É. PLESSIX, *An MSSS-preconditioned matrix equation approach for the time-harmonic elastic wave equation at multiple frequencies*, *Computational Geosciences*, 22 (2018), pp. 43–61.
- [5] M. BENZI, G. H. GOLUB, AND J. LIESEN, *Numerical solution of saddle point problems*, *Acta numerica*, 14 (2005), pp. 1–137.
- [6] M. BENZI AND M. A. OLSHANSKII, *An augmented lagrangian-based approach to the oseen problem*, *SIAM Journal on Scientific Computing*, 28 (2006), pp. 2095–2113.
- [7] J.-P. BERENGER, *A perfectly matched layer for the absorption of electromagnetic waves*, *Journal of computational physics*, 114 (1994), pp. 185–200.
- [8] J. BEZANSON, A. EDELMAN, S. KARPINSKI, AND V. B. SHAH, *Julia: A fresh approach to numerical computing*, *SIAM Review*, 59 (2017), pp. 65–98, <https://doi.org/10.1137/141000671>, <http://julialang.org/publications/julia-fresh-approach-BEKS.pdf>, <https://arxiv.org/abs/http://dx.doi.org/10.1137/141000671>.
- [9] B. BONEV AND J. S. HESTHAVEN, *A hierarchical preconditioner for wave problems in quasilinear complexity*, *SIAM Journal on Scientific Computing*, 44 (2022), pp. A198–A229.
- [10] A. BRANDT, *Multi-level adaptive solutions to boundary-value problems*, *Mathematics of com-*

- putation, 31 (1977), pp. 333–390.
- [11] A. BRANDT AND N. DINAR, *Multigrid solutions to elliptic flow problems*, in Numerical methods for partial differential equations, Elsevier, 1979, pp. 53–147.
 - [12] W. L. BRIGGS, V. E. HENSON, AND S. F. MCCORMICK, *A multigrid tutorial*, SIAM, second ed., 2000.
 - [13] J. CHEN, V. DWARKA, AND C. VUIK, *A matrix-free parallel two-level deflation preconditioner for two-dimensional heterogeneous helmholtz problems*, Journal of Computational Physics, 514 (2024), p. 113264.
 - [14] S. COOLS, P. GHYSELS, W. VAN AARLE, J. SIJBERS, AND W. VANROOSE, *A multi-level preconditioned krylov method for the efficient solution of algebraic tomographic reconstruction problems*, Journal of Computational and Applied Mathematics, 283 (2015), pp. 1–16.
 - [15] J.-C. N. ELEC, *Acoustic and electromagnetic equations: Integral representations for harmonic problems, vol. 44 of applied mathematical sciences*, 2001.
 - [16] H. ELMAN, V. E. HOWLE, J. SHADID, R. SHUTTLEWORTH, AND R. TUMINARO, *Block preconditioners based on approximate commutators*, SIAM Journal on Scientific Computing, 27 (2006), pp. 1651–1668.
 - [17] H. ELMAN, V. E. HOWLE, J. SHADID, R. SHUTTLEWORTH, AND R. TUMINARO, *A taxonomy and comparison of parallel block multi-level preconditioners for the incompressible navier–stokes equations*, Journal of Computational Physics, 227 (2008), pp. 1790–1808.
 - [18] H. ELMAN, V. E. HOWLE, J. SHADID, D. SILVESTER, AND R. TUMINARO, *Least squares preconditioners for stabilized discretizations of the navier–stokes equations*, SIAM Journal on Scientific Computing, 30 (2008), pp. 290–311.
 - [19] H. C. ELMAN, *Perturbation of eigenvalues of preconditioned navier–stokes operators*, SIAM Journal on Matrix Analysis and Applications, 18 (1997), pp. 733–751.
 - [20] H. C. ELMAN, *Preconditioning strategies for models of incompressible flow*, Journal of Scientific Computing, 25 (2005), pp. 347–366.
 - [21] H. C. ELMAN, O. G. ERNST, AND D. P. O’LEARY, *A multigrid method enhanced by krylov subspace iteration for discrete helmholtz equations*, SIAM Journal on scientific computing, 23 (2001), pp. 1291–1315.
 - [22] H. C. ELMAN, D. J. SILVESTER, AND A. J. WATHEN, *Finite elements and fast iterative solvers: with applications in incompressible fluid dynamics*, Oxford university press, 2014.
 - [23] H. C. ELMAN AND R. S. TUMINARO, *Boundary conditions in approximate commutator preconditioners for the navier–stokes equations*, Electronic Transactions on Numerical Analysis, 35 (2009), pp. 257–280.
 - [24] B. ENGQUIST AND A. MAJDA, *Absorbing boundary conditions for numerical simulation of waves*, Proceedings of the National Academy of Sciences, 74 (1977), pp. 1765–1766.
 - [25] Y. A. ERLANGGA, C. W. OOSTERLEE, AND C. VUIK, *A novel multigrid based preconditioner for heterogeneous helmholtz problems*, SIAM Journal on Scientific Computing, 27 (2006), pp. 1471–1492.
 - [26] M. J. GANDER AND H. ZHANG, *Domain decomposition methods for the Helmholtz equation: a numerical investigation*, in Domain Decomposition Methods in Science and Engineering XX, Springer, 2013, pp. 215–222.
 - [27] F. GASPAR, J. GRACIA, F. LISBONA, AND C. OOSTERLEE, *Distributive smoothers in multigrid for problems with dominating grad–div operators*, Numerical linear algebra with applications, 15 (2008), pp. 661–683.
 - [28] G. H. GOLUB AND C. GREIF, *On solving block-structured indefinite linear systems*, SIAM Journal on Scientific Computing, 24 (2003), pp. 2076–2092.
 - [29] D. GORDON AND R. GORDON, *Robust and highly scalable parallel solution of the Helmholtz equation with large wave numbers*, Journal of Computational and Applied Mathematics, 237 (2013), pp. 182–196.
 - [30] E. HABER AND S. MACLACHLAN, *A fast method for the solution of the Helmholtz equation*, J. Comput. Phys., 230 (2011), pp. 4403–4418.
 - [31] W. HACKBUSCH, *Multi-grid methods and applications*, vol. 4, Springer Science & Business Media, 2013.
 - [32] I. HARARI, M. SLAVUTIN, AND E. TURKEL, *Analytical and numerical studies of a finite element pml for the helmholtz equation*, Journal of Computational Acoustics, 8 (2000), pp. 121–137.
 - [33] F. H. HARLOW AND J. E. WELCH, *Numerical calculation of time-dependent viscous incompressible flow of fluid with free surface*, The physics of fluids, 8 (1965), pp. 2182–2189.
 - [34] E. HEIKKOLA, K. ITO, AND J. TOIVANEN, *A parallel domain decomposition method for the helmholtz equation in layered media*, SIAM Journal on Scientific Computing, 41 (2019), pp. C505–C521.
 - [35] I. C. IPSEN, *A note on preconditioning nonsymmetric matrices*, SIAM Journal on Scientific

- Computing, 23 (2001), pp. 1050–1051.
- [36] H. JOHNSTON AND J.-G. LIU, *Accurate, stable and efficient navier–stokes solvers based on explicit treatment of the pressure term*, Journal of Computational Physics, 199 (2004), pp. 221–259.
 - [37] D. KAY, D. LOGHIN, AND A. WATHEN, *A preconditioner for the steady-state navier–stokes equations*, SIAM Journal on Scientific Computing, 24 (2002), pp. 237–256.
 - [38] Y. LI, B. HAN, L. MÉTIVIER, AND R. BROSSIER, *Optimal fourth-order staggered-grid finite-difference scheme for 3d frequency-domain viscoelastic wave modeling*, Journal of Computational Physics, 321 (2016), pp. 1055–1078.
 - [39] I. LIVSHITS, *A scalable multigrid method for solving indefinite Helmholtz equations with constant wave numbers*, Numerical Linear Algebra with Applications, 21 (2014), pp. 177–193.
 - [40] G. S. MARTIN, R. WILEY, AND K. J. MARFURT, *Marmousi2: An elastic upgrade for marmousi*, The Leading Edge, 25 (2006), pp. 156–166.
 - [41] M. F. MURPHY, G. H. GOLUB, AND A. J. WATHEN, *A note on preconditioning for indefinite linear systems*, SIAM Journal on Scientific Computing, 21 (2000), pp. 1969–1972.
 - [42] L. N. OLSON AND J. B. SCHRODER, *Smoothed aggregation for Helmholtz problems*, Numerical Linear Algebra with Applications, 17 (2010), pp. 361–386.
 - [43] C. OOSTERLEE, C. VUIK, W. MULDER, AND R.-E. PLESSIX, *Shifted-laplacian preconditioners for heterogeneous Helmholtz problems*, in Advanced Computational Methods in Science and Engineering, Springer, 2010, pp. 21–46.
 - [44] J. W. PEARSON, *On the development of parameter-robust preconditioners and commutator arguments for solving stokes control problems*, Electronic Transactions on Numerical Analysis, 44 (2015), pp. 53–72.
 - [45] D. RABINOVICH, D. GIVOLI, AND E. BÉCACHE, *Comparison of high-order absorbing boundary conditions and perfectly matched layers in the frequency domain*, International Journal for Numerical Methods in Biomedical Engineering, 26 (2010), pp. 1351–1369.
 - [46] G. RIZZUTI AND W. A. MULDER, *Multigrid-based shifted-laplacian preconditioning for the time-harmonic elastic wave equation*, J. Comput. Phys., 317 (2016), pp. 47–65.
 - [47] J. RUDI, A. C. I. MALOSSI, T. ISAAC, G. STADLER, M. GURNIS, P. W. STAAR, Y. INEICHEN, C. BEKAS, A. CURIONI, AND O. GHATTAS, *An extreme-scale implicit solver for complex pdes: highly heterogeneous flow in earth’s mantle*, in Proceedings of the international conference for high performance computing, networking, storage and analysis, 2015, pp. 1–12.
 - [48] J. RUDI, G. STADLER, AND O. GHATTAS, *Weighted bfbt preconditioner for stokes flow problems with highly heterogeneous viscosity*, SIAM Journal on Scientific Computing, 39 (2017), pp. S272–S297.
 - [49] L. RUTHOTTO, E. TREISTER, AND E. HABER, *jinu—a flexible julia package for pde parameter estimation*, SIAM Journal on Scientific Computing, 39 (2017), pp. S702–S722.
 - [50] Y. SAAD, *A flexible inner-outer preconditioned gmres algorithm*, SIAM Journal on Scientific Computing, 14 (1993), pp. 461–469.
 - [51] D. SHIROKOFF AND R. R. ROSALES, *An efficient method for the incompressible navier–stokes equations on irregular domains with no-slip boundary conditions, high order up to the boundary*, Journal of Computational Physics, 230 (2011), pp. 8619–8646.
 - [52] D. SILVESTER, H. ELMAN, D. KAY, AND A. WATHEN, *Efficient preconditioning of the linearized navier–stokes equations for incompressible flow*, Journal of Computational and Applied Mathematics, 128 (2001), pp. 261–279.
 - [53] I. SINGER AND E. TURKEL, *A perfectly matched layer for the helmholtz equation in a semi-infinite strip*, Journal of Computational Physics, 201 (2004), pp. 439–465.
 - [54] C. C. STOLK, *A rapidly converging domain decomposition method for the Helmholtz equation*, J. Comput. Phys., 241 (2013), pp. 240–252.
 - [55] E. TREISTER AND R. YOVEL, *A hybrid shifted laplacian multigrid and domain decomposition preconditioner for the elastic helmholtz equations*, Journal of Computational Physics, 497 (2024), p. 112622.
 - [56] U. TROTTEMBERG, C. OOSTERLEE, AND A. SCHÜLLER, *Multigrid*, Academic Press, London and San Diego, 2001.
 - [57] P. TSUJI, J. POULSON, B. ENGQUIST, AND L. YING, *Sweeping preconditioners for elastic wave propagation with spectral element methods*, ESAIM: Mathematical Modelling and Numerical Analysis, 48 (2014), pp. 433–447.
 - [58] P. TSUJI AND R. TUMINARO, *Augmented amg-shifted laplacian preconditioners for indefinite Helmholtz problems*, Numerical Linear Algebra with Applications, 22 (2015), pp. 1077–1101.
 - [59] H. A. VAN DER VORST, *Bi-CGSTAB: A fast and smoothly converging variant of Bi-CG for*

- the solution of nonsymmetric linear systems*, SIAM Journal on scientific and Statistical Computing, 13 (1992), pp. 631–644.
- [60] B. WANG, D. CHEN, B. ZHANG, W. ZHANG, M. H. CHO, AND W. CAI, *Taylor expansion based fast multipole method for 3-d helmholtz equations in layered media*, Journal of Computational Physics, 401 (2020), p. 109008.
- [61] S. WANG, V. MAARTEN, AND J. XIA, *Acoustic inverse scattering via helmholtz operator factorization and optimization*, Journal of Computational Physics, 229 (2010), pp. 8445–8462.
- [62] S. WANG, V. MAARTEN, AND J. XIA, *On 3d modeling of seismic wave propagation via a structured parallel multifrontal direct helmholtz solver*, Geophysical Prospecting, 59 (2011), pp. 857–873.
- [63] R. YOVEL AND E. TREISTER, *Lfa-tuned matrix-free multigrid method for the elastic helmholtz equation*, SIAM Journal on Scientific Computing, (2024), pp. S1–S21.
- [64] L. ZEPEDA-NÚÑEZ AND L. DEMANET, *Nested domain decomposition with polarized traces for the 2d helmholtz equation*, SIAM Journal on Scientific Computing, 40 (2018), pp. B942–B981.
- [65] Y. ZHU, E. SIFAKIS, J. TERAN, AND A. BRANDT, *An efficient multigrid method for the simulation of high-resolution elastic solids*, ACM Transactions on Graphics, 29 (2010), p. 16.
- [66] M. ZUBELDIA, *Energy concentration and explicit sommerfeld radiation condition for the electromagnetic helmholtz equation*, Journal of Functional Analysis, 263 (2012), pp. 2832–2862.